

# ECOGRAPHY

## Review

### How environmental drivers of spatial synchrony interact

Daniel C. Reuman<sup>1</sup>, Max C. N. Castorani<sup>2</sup>, Kyle C. Cavanaugh<sup>3</sup>, Lawrence W. Sheppard<sup>4</sup>, Jonathan A. Walter<sup>2,5</sup> and Tom W. Bell<sup>6,7</sup>

<sup>1</sup>Department of Ecology and Evolutionary Biology and Center for Ecological Research, University of Kansas, Lawrence, KS, USA

<sup>2</sup>Department of Environmental Sciences, University of Virginia, Charlottesville, VA, USA

<sup>3</sup>Department of Geography, University of California, Los Angeles, CA, USA

<sup>4</sup>Marine Biological Association of the United Kingdom, Plymouth, UK

<sup>5</sup>Center for Watershed Sciences, University of California, Davis, CA, USA

<sup>6</sup>Department of Applied Ocean Physics and Engineering, Woods Hole Oceanographic Institution, Woods Hole, MA, USA

<sup>7</sup>Earth Research Institute, University of California, Santa Barbara, CA, USA

Correspondence: Daniel C. Reuman ([reuman@ku.edu](mailto:reuman@ku.edu))

Ecography

2023: e06795

doi: [10.1111/ecog.06795](https://doi.org/10.1111/ecog.06795)

Subject Editor: Timothy Keitt

Editor-in-Chief: Robert D. Holt

Accepted 2 June 2023



Spatial synchrony, the tendency for populations across space to show correlated fluctuations, is a fundamental feature of population dynamics, linked to central topics of ecology such as population cycling, extinction risk, and ecosystem stability. A common mechanism of spatial synchrony is the Moran effect, whereby spatially synchronized environmental signals drive population dynamics and hence induce population synchrony. After reviewing recent progress in understanding Moran effects, we here elaborate a general theory of how Moran effects of different environmental drivers acting on the same populations can interact, either synergistically or destructively, to produce either substantially more or markedly less population synchrony than would otherwise occur. We provide intuition for how this newly recognized mechanism works through theoretical case studies and application of our theory to California populations of giant kelp. We argue that Moran interactions should be common. Our theory and analysis explain an important new aspect of a fundamental feature of spatiotemporal population dynamics.

Keywords: Fourier, interactions, kelp, *Macrocystis pyrifera*, Moran effects, synchrony

## Introduction

Spatial synchrony, the tendency for geographically disjunct populations to show correlated fluctuations through time, is a fundamental feature of population dynamics, linked to important topics such as population cycling (Anderson et al. 2021), extinction risk (Ghosh et al. 2020c), and the stability of regional populations and ecosystem functioning (Wilcox et al. 2017). Though spatial synchrony (henceforth, *synchrony*) has been studied for decades in a wide variety of species ranging from viruses and plants to mammals, and at spatial scales ranging from centimeters to over 1000 km



[www.ecography.org](http://www.ecography.org)

Page 1 of 18

© 2023 The Authors. Ecography published by John Wiley & Sons Ltd on behalf of Nordic Society Oikos

This is an open access article under the terms of the Creative Commons Attribution License, which permits use, distribution and reproduction in any medium, provided the original work is properly cited.

(Liebhold et al. 2004), recent advances in statistical methods and improvements in data availability have led to several major advances in our understanding of synchrony and its causes and consequences. For instance, the timescale structure of synchrony is now known to be important (Keitt 2008, Sheppard et al. 2016, Desharnais et al. 2018, Sheppard et al. 2019), synchrony is now known to have a complex and pronounced geography (Defriez and Reuman 2017a,b, Walter et al. 2017, 2020), and patterns of synchrony are now known to be 'asymmetric in distribution tails' in a way that is important for system stability (Ghosh et al. 2020a,b, Walter et al. 2022). Synchrony is asymmetric in distribution tails when two positively associated (synchronous) variables are more (respectively, less) synchronous in the lower parts of their distributions than in the upper parts. Our ability to infer the causes of synchrony is much improved in recent years (Sheppard et al. 2016, 2019, Defriez and Reuman 2017b, Walter et al. 2017, Anderson et al. 2018), and there is also growing evidence that synchrony is changing as a newly recognized component of climate change (Defriez et al. 2016, Sheppard et al. 2016, Hansen et al. 2020). Distinct viewpoints on synchrony from population and community ecology are becoming integrated, leading to a more holistic understanding of the importance of synchrony for ecosystem stability (Wang and Loreau 2014). These new developments have led to an increasingly central role of the phenomenon of synchrony in many of the most important research topics in ecology.

Correlations between weather time series measured in different locations can induce synchrony between populations in those locations if the weather variables influence population processes. This mechanism, called the Moran effect, is now known to be one of the most important causes of synchrony. But the mechanism was originally proposed theoretically (Moran 1953), and decades passed during which it was considered difficult to distinguish this potential cause of synchrony from others (e.g. dispersal) in field systems. Synchrony has long been thought to have three causes: dispersal, and trophic interactions with a synchronous or mobile species, in addition to the Moran effect (Liebhold et al. 2004). However, using common past statistical approaches which focussed on declines in population correlations with distance, patterns of synchrony produced by each of these mechanisms are quite similar (Ranta et al. 1999, Liebhold et al. 2004, Abbott 2007, Walter et al. 2017); so examination of such patterns provides little or no traction for inferring the causes of synchrony. Early empirical papers demonstrating the Moran effect mechanism resorted to special cases where dispersal was impossible and predators were absent (Grenfell et al. 1998, Tedesco et al. 2004). Controlled experiments also confirmed that all three theorized mechanisms could be involved in synchrony (Vasseur and Fox 2009). Nevertheless, the problem of inferring specific mechanisms of synchrony in field systems was considered a challenge until recently.

Recent research has provided new statistical viewpoints which have, when sufficient data are available, essentially solved the problem of inference of the causes of synchrony

(including identifying specific Moran drivers), and the research has revealed the broad importance of Moran effects. Approaches based on spatial statistics produced inferences that precipitation and temperature Moran effects are important causes of synchrony of terrestrial (Defriez and Reuman 2017b) and marine (Defriez and Reuman 2017a) primary productivity. Another geographic approach, based on multiple regression of distance matrices (MRM), was used to infer that a precipitation Moran effect is a cause of synchrony for the spongy moth (Haynes et al. 2013). Geographic approaches to identifying causes of synchrony (Koenig et al. 2017, Walter et al. 2020, Bogdziewicz et al. 2021) have become widespread (Gouveia et al. 2016, Walter et al. 2017, Larsen et al. 2021). MRM approaches have also been used to identify dispersal as a cause of synchrony (Anderson et al. 2018), sometimes combined with genetic methods (Haynes and Walter 2022). Another class of methods exploits the time and timescale structure of synchrony. For instance, Allstadt et al. (2015) confirmed the importance of a precipitation Moran effect in spongy moth. A suite of wavelet and related Fourier techniques has been developed that can comprehensively describe the time and timescale structure of synchrony, identify Moran drivers of synchrony operating in distinct timescale bands, and apportion fractions of observed synchrony to respective Moran drivers (Sheppard et al. 2016, 2017, 2019, Desharnais et al. 2018, Anderson et al. 2021, Reuman et al. 2021).

The techniques reviewed above have made it possible for several recent papers to identify cases in which two or more distinct Moran drivers operate simultaneously on the same populations (Defriez and Reuman 2017b, Haynes et al. 2019, Walter et al. 2019, 2020, Anderson et al. 2021). In fact, two recent papers have documented that Moran effects of distinct environmental drivers can interact, either synergistically or antagonistically, so that total population synchrony can be either greater than or less than what synchrony would be if the distinct Moran drivers operated independently (Sheppard et al. 2019, Castorani et al. 2022). Sheppard et al. (2019) showed that long-timescale (>4-year period) synchrony in a chlorophyll density index in the seas around the United Kingdom is substantially augmented by interactions between environmental drivers of synchrony and drivers linked with consumption by a copepod consumer. Castorani et al. (2022) showed that nutrient dynamics and wave disturbance, two Moran drivers of synchrony in giant kelp populations on the California (CA) coast, interact either synergistically or destructively, depending on which portion of the CA coast is examined and on the timescale of analysis.

The main purpose of this study is to establish a general theory of the mechanism of interacting Moran effects and to use examples and applications of the theory to provide ecological intuition for how the mechanism of interacting Moran effects works. Our goals are distinct from those of Kendall et al. (2000), who examined interactions between Moran and dispersal causes of synchrony.

The basic fact that Moran drivers can interact, synergistically or destructively, can be demonstrated with a very simple

model which we now elaborate, though understanding the full nature of the interaction mechanism will require the rest of this paper. Suppose  $\varepsilon_i^{(1)}(t)$  and  $\varepsilon_i^{(2)}(t)$  are environmental random variables measured in locations  $i=1, 2$  at times  $t$ , and assume these are independent through time and standard normally distributed for all  $i$  and  $t$ . If a population index  $w_i(t)$  follows the autoregressive process  $w_i(t) = bw_i(t-1) + \varepsilon_i^{(1)}(t)$  for  $i=1, 2$ , then the classic Moran theorem (Moran 1953) implies that temporal population correlation equals temporal environmental correlation, i.e.  $\text{cor}(\varepsilon_1^{(1)}, \varepsilon_2^{(1)})$ . If, instead,  $w_i(t) = bw_i(t-1) + \varepsilon_i^{(1)}(t) + \varepsilon_i^{(2)}(t)$ , so that both environmental variables influence populations, the Moran theorem then implies that population synchrony is  $\text{cor}(\varepsilon_1^{(1)} + \varepsilon_1^{(2)}, \varepsilon_2^{(1)} + \varepsilon_2^{(2)})$ . As we show in detail in the Supporting information, it is straightforward to show that this quantity depends not only on the standard environmental synchrony measures  $\text{cov}(\varepsilon_1^{(1)}, \varepsilon_2^{(1)})$  and  $\text{cov}(\varepsilon_1^{(2)}, \varepsilon_2^{(2)})$ , but also on ‘cross synchrony’ measures such as  $\text{cov}(\varepsilon_1^{(1)}, \varepsilon_2^{(2)})$  and  $\text{cov}(\varepsilon_1^{(2)}, \varepsilon_2^{(1)})$ . Cross synchrony measures represent synchrony between an environmental variable in one location and a different variable in another location. Figure 1 illustrates, using this model, how population synchrony can therefore differ from what synchrony would be if the environmental processes  $\varepsilon^{(1)}$  and  $\varepsilon^{(2)}$  were unrelated. The difference is due to interactions between

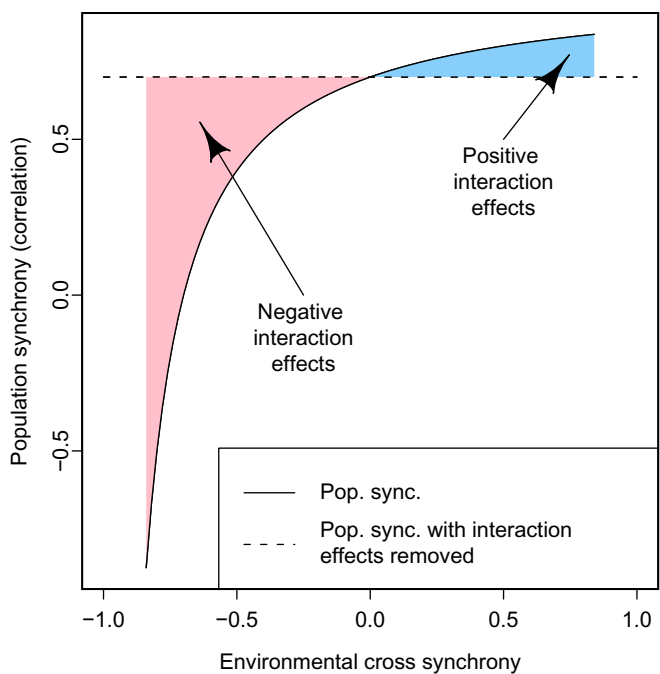


Figure 1. Example of interacting Moran effects. The example, which is based on the very simple model described in the Introduction, shows that interaction effects are possible, and can be substantially positive or negative. We used  $\text{cov}(\varepsilon_1^{(1)}, \varepsilon_2^{(1)}) = \text{cov}(\varepsilon_1^{(2)}, \varepsilon_2^{(2)}) = 0.7$ , and the values  $\text{cov}(\varepsilon_i^{(1)}, \varepsilon_j^{(2)})$ , for  $i, j = 1, 2$ , were all set equal to each other and the common value appears on the horizontal axis – cross synchrony of the environmental variables. See the online version for color renderings of all figures.

the two Moran effects, and can be substantially positive or negative. This example was adapted from Supporting information section S1 of Sheppard et al. (2019). All notation and abbreviations used throughout the paper are summarized in Table 1. Typesetting procedures used by publishers of ecological journals often render mathematical expressions sub-optimally, so we have appended to the end of the Supporting information a version of this main text which was rendered using latex. It is recommended that readers interested in the mathematical content of the study read that version.

Having demonstrated that interactions between Moran effects can occur, we now use a simple analogy from common experience to begin to provide intuition. Consider  $N$  children, each riding on their own playground swing and each being pushed both by their own mother and their own father. Here, the children correspond to ecological populations and the parental pushing to environmental influences on the populations. If the fathers from separate families were to synchronize their pushes, they would act as a Moran-like influence, tending to synchronize the swinging motions of the children. Likewise, if the mothers from separate families were to synchronize their pushes, it would tend to have a separate synchronizing effect. If the pushes of the fathers were appropriately coordinated with the pushes of the mothers (either happening at the same time, if the mothers and fathers are standing on the same sides of the swinging children, or at opposite times in the swing period if the parents are on opposite sides), the children would swing higher, and would also swing more synchronously, demonstrating a synergistic interaction between synchronizing effects, i.e. a tendency for the two synchronizing effects to reinforce each other. On the other hand, if the maternal and paternal pushes were not appropriately coordinated, the children would swing more or less randomly, with smaller amplitude, and would become asynchronous with each other. This second case demonstrates an antagonistic interaction between synchronizing effects, i.e. a tendency for the two synchronizing effects to cancel. As oscillators, children on swings are distinct in many ways from populations, not least because swings oscillate on one frequency/timescale, whereas populations typically oscillate simultaneously on many timescales. We will see that a key insight is the use of a timescale-specific approach. By timescale-specific, we mean that fluctuations having different characteristic periods, which are superimposed in actual population time series data, can be understood separately. Timescale-specific approaches have been shown to be important to understanding synchrony and other phenomena (Sheppard et al. 2016, Zhao et al. 2020, Anderson et al. 2021). In the approach used in this paper, environmental and population signals are decomposed using Fourier analysis. The simple swing analogy turns out to supply, in much idealized form, the basic intuition our formal theory will extend.

Both Sheppard et al. (2019) and Castorani et al. (2022) argued that interactions between Moran effects may be a general feature of many systems, because of the large number of interrelated factors driving population fluctuations in most spatially extended systems. The same two studies

Table 1. Summary of notation and abbreviations.

Notation	Meaning
$i=1, \dots, N$	Locations of population sampling
$t=1, \dots, T$	Times of population sampling
$w_i(t)$	A population index at location $i$ and time $t$
$\varepsilon_i^{(a)}(t)$	Environmental variable $a$ measured at location $i$ and time $t$
$l_{ek}$	Lag of the effects of environmental variable $k$ on populations
$l_n$	A lag between two environmental variables
$l_{e1} - l_{e2} + l_n$	The <i>environmental effect alignment measure</i>
$\sigma$	A timescale
$f=1/\sigma$	Frequency
$S_{w_i w_i}$	The power spectrum of the process $w_i$
$S_{w_i w_j}$	The cross spectrum of the processes $w_i$ and $w_j$
$S_{ww}$	The spectral matrix of the $N$ -dimensional process $w$
$\rho_{ww}$	Synchrony of the process $w$
$\rho_{\varepsilon^{(1)} \varepsilon^{(2)}}$	Cross synchrony of the processes $\varepsilon^{(1)}$ and $\varepsilon^{(2)}$
$b_1, \dots, b_n$	Autoregressive coefficients in the population model
$p_0^{(k)}, \dots, p_{m_k}^{(k)}$	Coefficients for the lagged effects of $\varepsilon^{(k)}$ on populations
$\delta$	Effects of unmeasured environmental variables
$\mu$	$\exp(-2\pi i \mu)$ for $i$ the imaginary unit
$f_B$	$1 - b_1 \mu - b_2 \mu^2 - \dots - b_n \mu^n$
$f_{p^{(k)}}$	$p_0^{(k)} + p_1^{(k)} \mu + \dots + p_{m_k}^{(k)} \mu^{m_k}$
$\frac{ f_{p^{(k)}} ^2}{ f_B ^2} \rho_{\varepsilon^{(k)} \varepsilon^{(k)}}$	Direct Moran effects of variable $k$ in the theory
$2\text{Re}(f_{p^{(1)}} \overline{f_{p^{(2)}}} \varepsilon^{(1)} \varepsilon^{(2)})$	Moran interactions
CaseA, CaseB, CaseC1, CaseC2	Names of theoretical case studies
CCA1	Region 1 of central California (Fig. 3)
CCA2	Region 2 of central California (Fig. 3)
SB	Region around Santa Barbara (Fig. 3)

demonstrated that interaction effects can be strong. For these reasons and others, development of a general theoretical and intuitive understanding of how interactions between Moran effects work is an important research goal. We explore in the Discussion why climate change may also influence Moran interactions, and we extend the arguments of Sheppard et al. (2019) and Castorani et al. (2022) that interactions between Moran effects are likely to be common.

Our specific goals for this study are as follows. First, (G1) we will elaborate a general theory of interacting Moran effects which allows a detailed understanding of how the mechanism works. Second, (G2) we will consider theoretical case studies, which emerge as important special cases of our general theory, and which illuminate the intuition behind how Moran effects may interact in real systems. Third, (G3) we will apply our theory to populations of giant kelp off the CA coast. Whereas Castorani et al. (2022) already carried out a detailed analysis of interacting Moran effects in CA kelp populations and their importance for kelp ecology, we instead use a simplified subset of the available kelp data. Our kelp results are not intended to extend what is known about kelp ecology (beyond what was discovered in our earlier paper, Castorani et al. 2022), but

rather serve as a vehicle for understanding the inner workings of our general theory of interacting Moran effects. Overall, this study introduces a general theory of Moran interactions and uses it to conceptually illuminate this newly observed but potentially quite important mechanism of spatiotemporal population dynamics.

## General theory

### Building intuition for Moran interactions: a single timescale

Prior to presenting our formal theory, we extend and formalize the intuition behind it that began with the swing analogy in the Introduction. We again focus on a single timescale of oscillation, later combining timescales mathematically. Figure 2a–b shows the period-20 Fourier components of two hypothetical, spatially synchronous environmental variables measured in sampling locations  $i=1, 2, 3$ , and one way these can influence populations. The components are lagged, relative to each other, in the timing of their peaks ( $l_n$  on the figure).

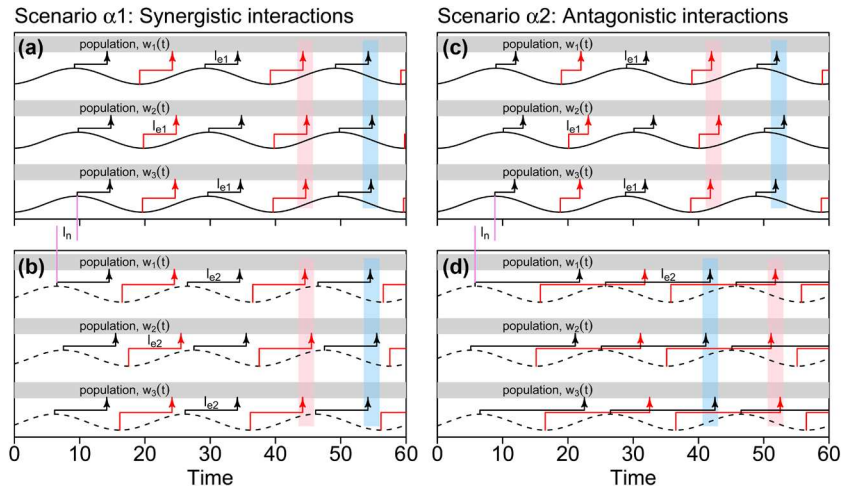


Figure 2. Illustration of the main concept of synergistically or antagonistically interacting Moran effects. Interactions require that each environmental variable itself be spatially synchronous; and then the alignment or misalignment of three types of lag determine the sign and strength of the interactions. Solid-line sinusoids represent the period-20 components of an environmental variable in three locations ( $\varepsilon_i^{(1)}$  for  $i = 1, 2, 3$ ) and dashed-line sinusoids represent the period-20 components of a different environmental variable in the same locations ( $\varepsilon_i^{(2)}$  for  $i = 1, 2, 3$ ). Black arrows represent peak positive influences of environmental variables on populations, which are lagged by an amount  $l_{e1}$  for  $\varepsilon_i^{(1)}$  and by an amount  $l_{e2}$  for  $\varepsilon_i^{(2)}$ , where these lags differ across the scenarios  $\alpha 1$  and  $\alpha 2$ , but are the same in all locations within one of these scenarios. Analogously, red arrows represent maximally negative effects. Due to environmental synchrony, peak positive population effects of the same variable occur at similar times across locations, and likewise for peak negative effects, illustrated with blue and pink rectangles. In the synergistic scenario ( $\alpha 1$ ), the lag between the environmental variables ( $l_n$ ) and the lags of the population effects of the variables ( $l_{e1}$  and  $l_{e2}$ ) are aligned, i.e. the *environmental effect alignment measure*,  $l_n + l_{e1} - l_{e2}$  (main text), equals zero. So peak positive effects of  $\varepsilon_i^{(1)}$  coincide with peak positive effects of  $\varepsilon_i^{(2)}$  (the pink rectangles are aligned on a, b), augmenting synchrony. Likewise, negative effects are aligned (blue rectangles). In the antagonistic scenario ( $\alpha 2$ ), lags are misaligned, i.e.  $l_n + l_{e1} - l_{e2} = -\sigma/2$ , where  $\sigma = 20$  is the period. So peak positive effects of  $\varepsilon_i^{(1)}$  coincide with maximally negative effects of  $\varepsilon_i^{(2)}$ , and maximally negative effects of  $\varepsilon_i^{(1)}$  coincide with peak positive effects of  $\varepsilon_i^{(2)}$  (pink rectangles on c are aligned with blue ones on d, and vice versa), reducing synchrony. See the online version for color renderings of all figures.

They are also lagged in their effects on populations, by the amounts  $l_{e1}$  and  $l_{e2}$ , respectively, i.e. peaks in the environmental signals manifest as maximum positive influence on populations after delays of  $l_{e1}$  and  $l_{e2}$ , respectively. Such delays can be due to a variety of biological mechanisms associated with the life history of the organisms which comprise the populations. In this example, we assume for simplicity that larger values of both environmental variables are beneficial to populations, though the general theory described below does not require that assumption, and see also the next example which makes a different assumption. If, as in Fig. 2a–b,  $l_{e1} - l_{e2} + l_n = 0$  (or  $l_{e1} - l_{e2} + l_n$  is any integer multiple of  $\sigma = 20$ , the period), then the periodic maximal positive influences of the two environmental variables coincide with each other as well as being spatially synchronous. This alignment of influences produces additional synchrony in populations, beyond what would manifest if environmental fluctuations were unrelated, because positive influences of variable 1 in location  $i$  will tend to coincide with positive influences of variable 2 in location  $j$ . In contrast, Fig. 2c–d shows the opposite scenario, for which  $l_{e1} - l_{e2} + l_n = -\sigma/2$ . Thus the periodic maximal positive influence of environmental variable 1 coincides with the periodic maximal negative influence of

environmental variable 2, reducing synchrony relative to the case of unrelated environmental variables. (The same outcome would occur if  $l_{e1} - l_{e2} + l_n$  were any integer multiple of  $\sigma$  plus or minus  $\sigma/2$ .) Intermediate scenarios between the two scenarios of Fig. 2 are also possible, as will be revealed by our theory. We henceforth refer to the quantity  $l_{e1} - l_{e2} + l_n$  as the *environmental effect alignment measure*, because it measures the extent to which the timing of the population influences of the two environmental variables are aligned. If we replace the assumption that larger values of both environmental variables are beneficial to populations with an assumption that larger values of the first variable and smaller values of the second are beneficial, scenarios of synergistic versus antagonistic Moran interactions are reversed, but with the same general concepts still operating (Supporting information analogue of Fig. 2).

### Formal theory

Our formal theory requires a conceptual understanding of the *spectrum* of an environmental or population time series, as well as of the *cospectrum* and *cross spectrum* of two time series, so we briefly introduce these concepts. If  $w_i(t)$  is a

stochastic process or time series measured at location  $i$  (e.g. the population density time series of a species of interest in that location), the spectrum  $S_{w_i w_i}(f)$  is a function of frequency,  $f$ . For a periodic oscillation,  $f$  can be defined as one over the timescale, or period,  $\sigma$ , of the oscillation. The spectrum  $S_{w_i w_i}(f)$  is larger for frequencies at which  $w_i(t)$  oscillates with larger amplitude. So, for example, a population  $w_i(t)$  that shows strong oscillatory dynamics of five-year period will have a large value of  $S_{w_i w_i}(f)$  for  $f = \frac{1}{5} \text{y}^{-1}$ .

The spectrum separates the overall variance of a time series into contributions which occur at different frequencies, in the sense that an integral of  $S_{w_i w_i}(f)$  across all frequencies equals  $\text{var}(w_i)$ . In a similar way, the cospectrum of two time series,  $w_i(t)$  and  $w_j(t)$ , is a function of  $f$  that takes large values at frequencies for which oscillations in  $w_i(t)$  and  $w_j(t)$  are both strong and strongly correlated, i.e. they have the same or similar phase. Here,  $j$  refers to another location where measurements were taken. The cospectrum is the real part of the cross spectrum,  $S_{w_i w_j}(f)$ , which is a complex-valued function of frequency. The cross-spectrum takes large-magnitude values at frequencies,  $f$ , for which the oscillatory components of  $w_i(t)$  and  $w_j(t)$  are strong and in a consistent phase relationship to each other; and the complex phase of the cross spectrum at  $f$  then quantifies that relationship. The notation  $S_{w w}(f)$  refers to the *spectral matrix*, which has  $ij$ th entry  $S_{w_i w_j}(f)$ . The notation  $S_{w_i w_i}$  for the spectrum makes sense and is consistent with the notation  $S_{w_i w_j}$  for the cross spectrum because the spectrum of  $w_i$  is the cross spectrum of  $w_i$  with itself. Spectral methods are standard (Vasseur and Gaedke 2007, Defriez and Reuman 2017a,b), and many background references are available (Brillinger 2001).

Much prior work demonstrates the importance of a frequency- or timescale-specific approach to synchrony (Vasseur and Gaedke 2007, Keitt 2008, Defriez et al. 2016, Sheppard et al. 2016, Desharnais et al. 2018, Anderson et al. 2021; frequency- and timescale-specific approaches are equivalent because frequency and timescale are reciprocal), and it will turn out (below and Discussion) that a timescale-specific approach is essential to the development of our new theory. We therefore here define, using the spectral methods outlined above, a frequency/timescale-specific measure of synchrony, as well as a new concept of *cross-variable synchrony*. If time series data  $w_i(t)$  for  $t=1,\dots,T$  were gathered at locations  $i=1,\dots,N$ , our synchrony measure is simply  $\rho_{ww} = \left( \sum_{i \neq j} S_{w_i w_j} \right) / (N^2 - N)$ , the average of the cross spectra for all pairs of distinct locations. This is a real-valued function of frequency, an integral (across frequencies) of which is the classic, non-frequency-specific synchrony measure  $\left( \sum_{i \neq j} \text{cov}(w_i, w_j) \right) / (N^2 - N)$  (see Supporting information for details, here, and additional comparisons to previous measures of synchrony). Because  $\rho_{ww}$  is a real-valued function of frequency, it equals

$\rho_{ww} = \text{Re}(\rho_{ww}) = \left( \sum_{i \neq j} \text{Re}(S_{w_i w_j}) \right) / (N^2 - N)$ , which only involves the cospectrum,  $\text{Re}(S_{w_i w_j})$ , not the full cross-spectrum,  $S_{w_i w_j}$ . If two time series  $\varepsilon_i^{(1)}(t)$  and  $\varepsilon_i^{(2)}(t)$  (e.g. two environmental variables) were measured at each sampling location and time, cross-variable synchrony (or, simply, *cross synchrony*) between the variables is defined as  $\rho_{\varepsilon^{(1)} \varepsilon^{(2)}} = \left( \sum_{i \neq j} S_{\varepsilon_i^{(1)} \varepsilon_j^{(2)}} \right) / (N^2 - N)$ . This is interpretable as pertaining to spatial synchrony because it makes comparisons across distinct locations. It is interpretable as cross-variable synchrony because comparisons are between the two variables, i.e. cross spectra between time series components of  $\varepsilon^{(1)}$  and  $\varepsilon^{(2)}$  are used. The new index takes into account possible time lags. For instance, if both  $\varepsilon^{(1)}$  and  $\varepsilon^{(2)}$  show strong, spatially synchronous, four-year-period oscillations, but peaks in the  $\varepsilon^{(2)}$  oscillations consistently lag peaks in the  $\varepsilon^{(1)}$  oscillations by a year, then  $\rho_{\varepsilon^{(1)} \varepsilon^{(2)}}$ , which is complex valued, will have high magnitude at timescale 4y, equivalent to frequency  $f = \frac{1}{4} \text{y}^{-1}$ , and will have phase at that frequency equal to  $\pi/2$ , reflecting the one-year lag. See Supporting information for detailed examples of cross synchrony.

Our population model is

$$w_i(t) = b_1 w_i(t-1) + \dots + b_n w_i(t-n) \quad (1)$$

$$+ p_0^{(1)} \varepsilon_i^{(1)}(t) + \dots + p_{m_1}^{(1)} \varepsilon_i^{(1)}(t-m_1) \quad (2)$$

$$+ p_0^{(2)} \varepsilon_i^{(2)}(t) + \dots + p_{m_2}^{(2)} \varepsilon_i^{(2)}(t-m_2) \quad (3)$$

$$+ \delta_i(t), \quad (4)$$

where  $w_i(t)$  is an index of the population in location  $i=1,\dots,N$  at time  $t$ , and  $\varepsilon^{(1)} = (\varepsilon_1^{(1)}, \dots, \varepsilon_N^{(1)})$ ,  $\varepsilon^{(2)} = (\varepsilon_1^{(2)}, \dots, \varepsilon_N^{(2)})$  and  $\delta = (\delta_1, \dots, \delta_N)$  are environmental processes at the same locations. The processes  $\varepsilon^{(1)}$  and  $\varepsilon^{(2)}$  are taken to be measured, whereas  $\delta$  represents the aggregate influence of unmeasured processes. We assume that the combined process  $(\varepsilon_1^{(1)}, \dots, \varepsilon_N^{(1)}, \varepsilon_1^{(2)}, \dots, \varepsilon_N^{(2)}, \delta_1, \dots, \delta_N)$  is an ergodic second-order stationary stochastic process (Brillinger 2001) with expected values of its components equal to zero. We make additional mild regularity assumptions for model stability, detailed in the Supporting information. Our model can be seen as a linearization of a very general dynamical model, influenced by 'weak noise' (see, e.g., Supporting information section S1.2 of Desharnais et al. 2018 and Supporting information section S1 of Walter et al. 2017). Linearization and 'weak noise' assumptions have been commonly adopted to make theoretical progress in ecology, and it has been demonstrated that results based on a weak noise assumption often hold for noise which is fairly strong (Nisbet et al. 1977, Desharnais et al. 2018). The topic of nonlinearity is revisited in the

Discussion. See [Brillinger \(2001\)](#) for background on stochastic processes.

Fulfilling goal G1 of the Introduction (i.e. to elaborate theory of interacting Moran effects), the outcome of our theory is an equation that expresses population synchrony in terms of synchrony of the environmental processes  $\varepsilon^{(1)}$  and  $\varepsilon^{(2)}$ , and cross synchrony between those processes:

$$\rho_{ww} = \frac{1}{|f_B|^2} \left[ |f_{\mathcal{P}^{(1)}}|^2 \rho_{\varepsilon^{(1)}\varepsilon^{(1)}} + |f_{\mathcal{P}^{(2)}}|^2 \rho_{\varepsilon^{(2)}\varepsilon^{(2)}} + 2\operatorname{Re}\left(f_{\mathcal{P}^{(1)}} \overline{f_{\mathcal{P}^{(2)}}} \rho_{\varepsilon^{(1)}\varepsilon^{(2)}}\right) \right] \quad (5)$$

$$+ \text{other contributions.} \quad (6)$$

Here,  $f_{\mathcal{P}^{(1)}} = p_0^{(1)} + p_1^{(1)}\mu + \dots + p_{m_1}^{(1)}\mu^{m_1}$ ,  $f_{\mathcal{P}^{(2)}} = p_0^{(2)} + p_1^{(2)}\mu + \dots + p_{m_2}^{(2)}\mu^{m_2}$ , where  $\mu = \exp(-2\pi i f)$ , and where  $i$ , the Greek letter iota, is the imaginary unit. The derivation of the theory is in Supporting information, where additional perspectives on our theory can also be found.

Comparing the terms on the right of (5) gives the relative contributions of direct Moran effects and interactions between Moran effects. The first term on the right of (5) is the component of population synchrony due to the direct Moran effects of  $\varepsilon^{(1)}$ , the second term is the component due to the direct Moran effects of  $\varepsilon^{(2)}$ , and the third term is the component due to interactions between the Moran effects of the two drivers. The ‘other contributions’ above correspond to synchronizing influences of  $\delta$  and of interactions between  $\delta$  and the  $\varepsilon^{(i)}$ . Such contributions would be difficult to assess because  $\delta$  was unmeasured.

The way direct Moran effects in our theory are interpreted is fairly straightforward. The magnitudes of the quantities  $f_{\mathcal{P}^{(1)}}$  and  $f_{\mathcal{P}^{(2)}}$  quantify the strength of influence of  $\varepsilon^{(1)}$  and  $\varepsilon^{(2)}$  on populations at the timescale  $\sigma = 1/f$ . The direct Moran effect term in (5) for  $\varepsilon^{(1)}$ , i.e.  $|f_{\mathcal{P}^{(1)}}|^2 \rho_{\varepsilon^{(1)}\varepsilon^{(1)}} / |f_B|^2$ , equals the synchrony of the  $\varepsilon^{(1)}$  time series themselves,  $\rho_{\varepsilon^{(1)}\varepsilon^{(1)}}$ , times the timescale-specific strength of influence of  $\varepsilon^{(1)}$  on the populations,  $|f_{\mathcal{P}^{(1)}}|^2$ , and modulated by the autoregressive nature of population dynamics,  $1/|f_B|^2$ . The term for the direct Moran effects of  $\varepsilon^{(2)}$  is interpreted similarly.

The components of the interacting Moran effects term in our theory are also interpretable. The phases of the quantities  $f_{\mathcal{P}^{(1)}}$  and  $f_{\mathcal{P}^{(2)}}$  quantify the lags in the population influences of  $\varepsilon^{(1)}$  and  $\varepsilon^{(2)}$ , represented on [Fig. 2](#) by  $l_{e1}$  and  $l_{e2}$ , relative to the timescale  $\sigma = 1/f$ . The lag  $l_n$  on [Fig. 2](#) manifests in the theory through the phase of  $\rho_{\varepsilon^{(1)}\varepsilon^{(2)}}$ . The environmental effect alignment measure,  $l_{e1} - l_{e2} + l_n$ , corresponds to the phase of the expression  $f_{\mathcal{P}^{(1)}} \overline{f_{\mathcal{P}^{(2)}}} \rho_{\varepsilon^{(1)}\varepsilon^{(2)}}$ , because the phase of this product equals the phase of  $f_{\mathcal{P}^{(1)}}$  (which corresponds to  $l_{e1}$ ), minus the phase of  $f_{\mathcal{P}^{(2)}}$  (which corresponds to  $l_{e2}$ ), plus the phase of  $\rho_{\varepsilon^{(1)}\varepsilon^{(2)}}$  (which corresponds to  $l_n$ ). The real part of  $f_{\mathcal{P}^{(1)}} \overline{f_{\mathcal{P}^{(2)}}} \rho_{\varepsilon^{(1)}\varepsilon^{(2)}}$  is positive whenever the phase of this quantity is close to zero, e.g. when environmental influences are positive and  $l_{e1} - l_{e2} + l_n$  is close to zero ([Fig. 2a–b](#)); and is increasingly negative as the phase of  $f_{\mathcal{P}^{(1)}} \overline{f_{\mathcal{P}^{(2)}}} \rho_{\varepsilon^{(1)}\varepsilon^{(2)}}$  gets close to  $\pi$ , e.g. when  $l_{e1} - l_{e2} + l_n$  is close to  $-\sigma/2$  ([Fig. 2c–d](#)). The factor  $1/|f_B|^2$  again captures how the intrinsic nature of population dynamics modulates Moran influences.

plus the phase of  $\rho_{\varepsilon^{(1)}\varepsilon^{(2)}}$  (which corresponds to  $l_n$ ). The real part of  $f_{\mathcal{P}^{(1)}} \overline{f_{\mathcal{P}^{(2)}}} \rho_{\varepsilon^{(1)}\varepsilon^{(2)}}$  is positive whenever the phase of this quantity is close to zero, e.g. when environmental influences are positive and  $l_{e1} - l_{e2} + l_n$  is close to zero ([Fig. 2a–b](#)); and is increasingly negative as the phase of  $f_{\mathcal{P}^{(1)}} \overline{f_{\mathcal{P}^{(2)}}} \rho_{\varepsilon^{(1)}\varepsilon^{(2)}}$  gets close to  $\pi$ , e.g. when  $l_{e1} - l_{e2} + l_n$  is close to  $-\sigma/2$  ([Fig. 2c–d](#)). The factor  $1/|f_B|^2$  again captures how the intrinsic nature of population dynamics modulates Moran influences.

## Material and methods

### Theoretical case studies

We now describe how we pursue goal G2 of the Introduction, to develop three theoretical case studies that illuminate the intuition of interacting Moran effects. For all cases, the model time step was assumed to be one quarter (q), i.e. four time steps per year. This makes no real mathematical difference, but was done to facilitate later comparisons with results for kelp data, which were sampled quarterly. For case study A (henceforth CaseA), the environmental variable  $\varepsilon^{(1)}$  is assumed to have a simple positive effect on populations, but lagged by one model time step (1q). For case study B (henceforth CaseB),  $\varepsilon^{(1)}$  is again assumed to have a simple positive effect on populations, but now lagged by 3q. For both CaseA and CaseB, the effects of  $\varepsilon^{(2)}$  are assumed to be un-lagged and positive. For case study C (CaseC), the effects of  $\varepsilon^{(1)}$  are positive and lagged by 1q and the effects of  $\varepsilon^{(2)}$  are unlagged and negative. The noise process ( $\varepsilon^{(1)}, \varepsilon^{(2)}$ ) is assumed to be a Gaussian white-noise process for both CaseA and CaseB. So the random variables  $(\varepsilon^{(1)}(t), \varepsilon^{(2)}(t))$  are independent and identically distributed (iid) for distinct times,  $t$ . Noise was positively correlated across space, and the components of  $\varepsilon^{(1)}(t)$  were positively correlated with those of  $\varepsilon^{(2)}(t)$ . For CaseC, the noise processes  $\varepsilon^{(1)}$  and  $\varepsilon^{(2)}$  are each assumed to exhibit spatially synchronous periodic oscillations of period one year, i.e. four model time steps, but with different phases. Peaks in  $\varepsilon^{(1)}$  are assumed to either lead or lag peaks in  $\varepsilon^{(2)}$  by 1q (we consider two sub-cases, CaseC1 and CaseC2). Such a situation could be realized by annually periodic environmental fluctuations sampled quarterly, e.g. wave action in central CA peaks annually in the winter, whereas surface-water nitrate concentrations also fluctuate with period one year, but peak in the spring, a delay of 1q compared to the wave peak. For all case studies, the autoregressive order of population dynamics is assumed, for simplicity, to be one. Details of the noise processes are in the Supporting information in the same section that has cross synchrony examples. Model coefficients and other setup details for the theoretical case studies are also specified in the Supporting information. Our case studies do not cover the full range of possible scenarios which can be illuminated by our general theory; they were selected

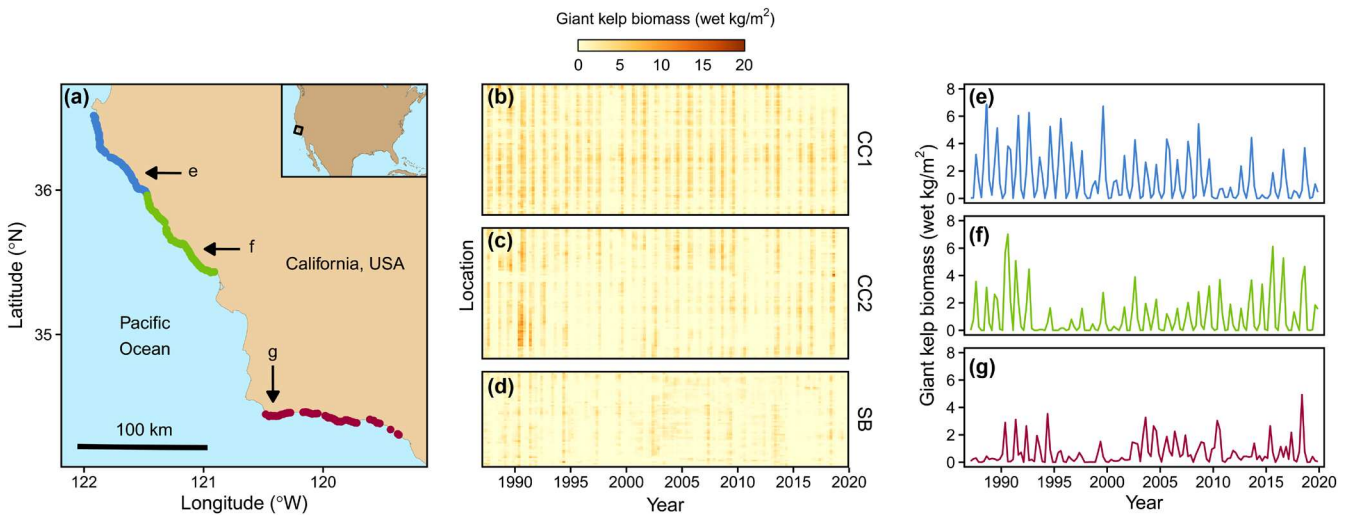


Figure 3. Kelp sampling sites and example time series. Sampling sites (a) were from three regions, central California 1 (CCA1, blue points), central California 2 (CCA2, green points) and the region around Santa Barbara (SB, red points). Kelp density in 500 m coastline segments is shown with color intensity in (b)–(d), and those panels correspond to the regions. One example time series from each region is shown in (e)–(g), with locations at which these time series were measured labeled on panels (a)–(d). See the online version for color renderings of all figures.

for the intuition they provide, and for the correspondence of some of the cases to the kelp examples we later discuss.

## Kelp examples

To help illustrate our theory, for goal G3 of the Introduction, we also apply the theory to an exceptional dataset on giant kelp (*Macrocystis pyrifera*) dynamics off the CA coast, and associated environmental measurements. The data are based on a subset of those used by [Castorani et al. \(2022\)](#) and [Walter et al. \(2022\)](#), and data details are given in those papers and in Supporting information; [Castorani et al. \(2022\)](#) and [Walter et al. \(2022\)](#) also provide an introduction to kelp ecology, and information on why giant kelp is an excellent species for studies of synchrony. We here summarize the format of the data after a preparation and cleaning process was implemented. After preparation, kelp data consisted of 224 quarterly kelp abundance time series from locations along the CA coast, each time series spanning from quarter 1 of 1987 to quarter 4 of 2019. Time series were grouped into three regions which were analyzed separately: a more northerly central CA group of 82 locations (called CCA1); a more southerly central CA group of 82 locations (CCA2); and a group of 60 locations from southern CA, close to Santa Barbara (called SB; [Fig. 3](#)). Each kelp measurement is an estimate of mean quarterly kelp canopy biomass (kg wet) per unit useable habitat ( $\text{m}^2$ ) along a 500 m stretch of coastline. We used coastline segments where kelp was persistent through essentially all of the 1987–2019 period (Supporting information). We also had estimates of maximum wave height and mean nitrate concentration for each quarter and location. Both waves and nutrients influence kelp dynamics and synchrony ([Cavanaugh et al. 2013](#), [Castorani et al. 2022](#)).

Coefficients of the model (1)–(4) were separately selected for each of our three regions using linear regression methods and building on extensive prior work on the drivers of kelp dynamics. A no-intercept regression model of kelp at time  $t$  in location  $i$ , i.e.  $w_i(t)$  in (1), against lagged values of kelp ( $w_i(t-l)$  for  $l=1,\dots,n$  in (1)), lagged and unlagged values of nitrates ( $\varepsilon_i^{(1)}(t-l)$  for  $l=0,\dots,m_1$  in (2)), and values of waves ( $\varepsilon_i^{(2)}(t-l)$  for  $l=0,\dots,m_2$  in (3)) was fitted using standard regression methods. The same regression coefficients were used for all locations within a region. Here, the  $w_i$  represent linearly detrended kelp time series in one of our regions,  $\varepsilon_i^{(1)}$  were detrended nitrate time series in the region, and  $\varepsilon_i^{(2)}$  were detrended wave disturbance time series. Waves influence kelp dynamics through direct disturbance events which can damage kelp or extirpate kelp locally when waves are large ([Cavanaugh et al. 2011](#), [Bell et al. 2015](#), [Schiel and Foster 2015](#)). Thus wave effects are immediate and  $m_2=0$  was used. Nitrates are known to fuel rapid kelp growth, though in some areas effects appear delayed by about 1q because our kelp data quantify canopy (surface) biomass, and it can take time for subsurface kelp to grow back to the surface ([Cavanaugh et al. 2011](#), [Bell et al. 2015](#), [Schiel and Foster 2015](#)). Therefore  $m_1=1$  was used. Kelp holdfasts on the sea floor can last for multiple years, so kelp lag effects were considered: we used  $n=4,8,12q$  in separate analyses, with this choice making no substantive difference to results (Results). Fitted regression coefficients determined the quantities  $b_1,\dots,b_n$ ,  $p_0^{(1)}$ ,  $p_1^{(1)}$ , and  $p_0^{(2)}$  in (1)–(3), and therefore  $f_B$ ,  $f_{P^{(1)}}$  and  $f_{P^{(2)}}$  in (5), for each of our three regions.

To estimate the components  $\rho_{ww}$ ,  $\rho_{\varepsilon^{(1)}\varepsilon^{(1)}}$ ,  $\rho_{\varepsilon^{(2)}\varepsilon^{(2)}}$  and  $\rho_{\varepsilon^{(1)}\varepsilon^{(2)}}$  in (5), we applied the definitions of these quantities (General Theory), which required estimation from

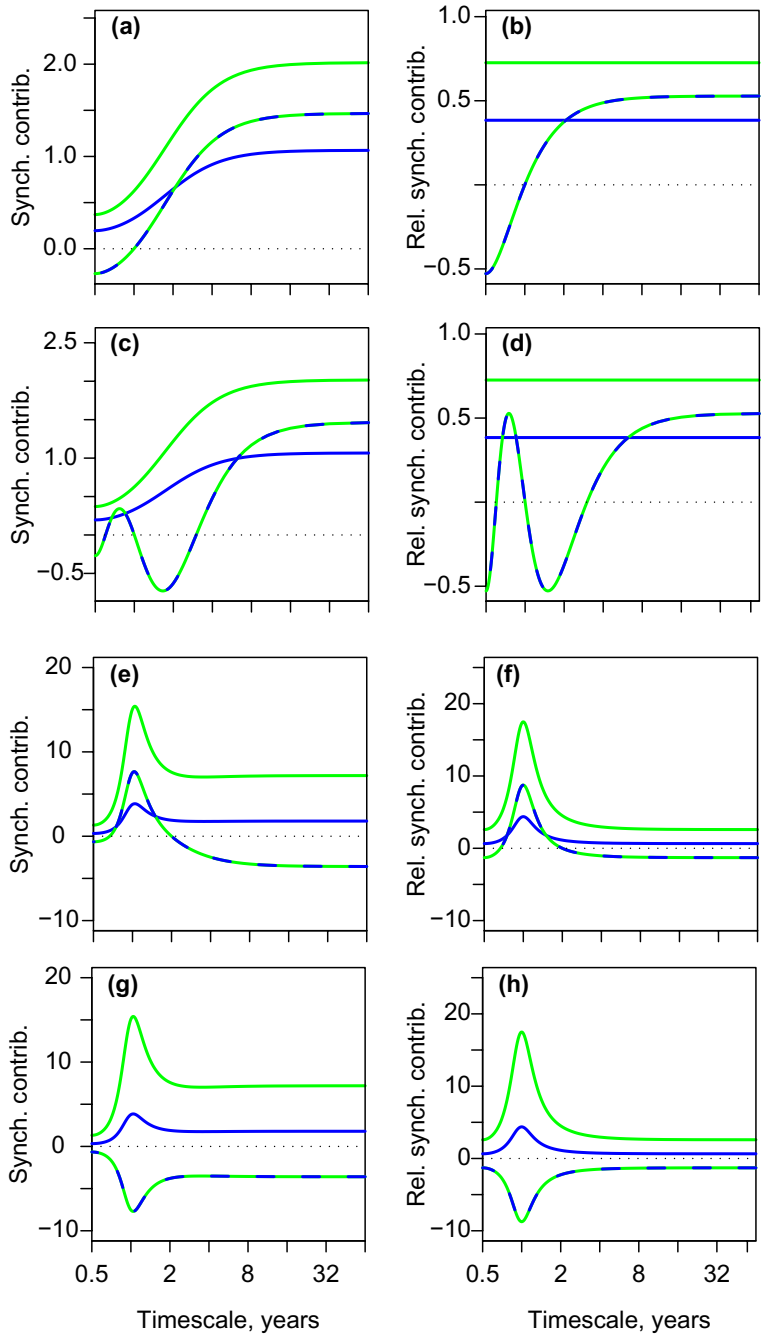


Figure 4. Results from theoretical case studies A (panels a–b), B (c–d), C1 (e–f) and C2 (g–h). Left panels (a, c, e, g) show the terms on the right side of (5). On those panels, the green line is  $\frac{|f_{\mathcal{P}^{(1)}}|^2}{|f_B|^2} \rho_{\varepsilon^{(1)} \varepsilon^{(1)}}$ , quantifying population synchrony due to the direct Moran effects of  $\varepsilon^{(1)}$ . The blue line is  $\frac{|f_{\mathcal{P}^{(2)}}|^2}{|f_B|^2} \rho_{\varepsilon^{(2)} \varepsilon^{(2)}}$ , quantifying population synchrony due to the direct Moran effects of  $\varepsilon^{(2)}$ . The dashed line is  $\frac{2\text{Re}(f_{\mathcal{P}^{(1)}} \overline{f_{\mathcal{P}^{(2)}}} \rho_{\varepsilon^{(1)} \varepsilon^{(2)}})}{|f_B|^2}$ , quantifying population synchrony due to interacting Moran effects. The functions plotted on b, d, f, h are those on a, c, e, g, respectively, times  $|f_B|^2$ , plotted to illustrate how autoregressive population effects modulate synchrony [see (5)]. For C1, peaks in the periodic noise process  $\varepsilon^{(2)}$  lagged peaks in the periodic process  $\varepsilon^{(1)}$  by 1 quarter (e–f), and for C2,  $\varepsilon^{(1)}$  lagged  $\varepsilon^{(2)}$  by the same amount (g–h). Synch. contrib. = Synchrony contribution refers to contributions to synchrony of the individual terms in our theory; Rel. synch. contrib. = Relative synchrony contribution refers to contributions expressed without accounting for the influence of autoregressive population effects. See the online version for color renderings of all figures.

data of the spectra and cross spectra  $S_{w_i w_j}$  and  $S_{\epsilon_i^{(a)} \epsilon_j^{(b)}}$  for  $i, j = 1, \dots, N$  and  $a, b = 1, 2$ , where  $N$  is the number of locations in the region being considered. Spectral quantities were computed using the consistent estimator of section 7.4 of Brillinger (2001). The estimator is a smoothed periodogram, with the width of the smoothing kernel selected to increase with the square root of time series length. Theory was interpreted in relation to kelp ecology and theoretical case studies by plotting the components of (5) for each of our regions.

Data for the project are publicly archived (Bell et al. 2021). All computations were done in R ver. 3.6.3 ([www.r-project.org](http://www.r-project.org)) on a laptop running Ubuntu Linux 16.04. Complete codes for the project workflow are at <https://github.com/reumanndc/InteractingMoranEffects>.

## Results

### Illustrating properties of Moran interactions: case studies

To begin fulfilling goal G2 of the Introduction, our theoretical case studies demonstrate that interaction effects between Moran drivers: 1) can be comparable in strength to direct Moran effects; 2) can be either synergistic or destructive; and 3) can depend strongly on timescale. First, for all of our case studies, the magnitude of interaction effects was comparable to that of direct Moran effects (Fig. 4, compare the dashed and solid lines). Thus interactions can contribute substantially to overall synchrony. Second, in contrast to direct Moran effects, which are positive, interactions can be negative or positive. CaseA and CaseB showed negative interaction effects on short timescales (Fig. 4a,c); CaseC1 showed negative interactions on long timescales (Fig. 4e); and CaseC2 showed negative interactions on all timescales (Fig. 4g). Thus interaction effects can either augment or reduce synchrony. Finally, interaction effects depended strongly on timescale for all case studies. This result complements earlier studies that showed direct Moran effects can depend on timescale (Defriez et al. 2016, Sheppard et al. 2016, Desharnais et al. 2018, Anderson et al. 2021). The results of this paragraph also follow from Sheppard et al. (2019) and Castorani et al. (2022), though not straightforwardly, and those papers are case studies, whereas our results provide general theory. See Supporting information for mathematical details of the theoretical case studies.

### Building intuition for Moran interactions: case studies

CaseA helps provide an intuitive understanding about how lags in Moran drivers can produce contrasting interactions between Moran effects on different timescales, and how our theory captures that contrast. For CaseA,  $\epsilon^{(1)}$  effects on populations were lagged by 1q but  $\epsilon^{(2)}$  effects were unlagged

(Methods). So, in the language of Fig. 2,  $l_{e1} = 1q$  and  $l_{e2} = 0q$ . The between-noise lag,  $l_n$ , of Fig. 2 is 0q because  $(\epsilon^{(1)}, \epsilon^{(2)})$  was taken to be a white noise process (Methods). Thus, the environmental effect alignment measure,  $l_{e1} - l_{e2} + l_n$ , equals 1q. What determines the sign of interactions between Moran effects for this example is how this measure compares to the timescale/period,  $\sigma$ , being considered. On the shortest timescales ( $\sigma = 0.5y = 2q$ ; Fig. 4a, left side of panel), 1q is half the period, so interaction effects are negative. On long timescales (e.g.  $\sigma > 8y$ ), 1q is a negligible portion of the period, so  $l_{e1} - l_{e2} + l_n$  is close to zero, relative to that period, and interaction effects are positive: relative to long timescales,  $\epsilon^{(1)}$  and  $\epsilon^{(2)}$  effects happen close to simultaneously, so the two noise variables reinforce each other. Comparing Fig. 4a–b shows the additional influence of autoregressive population effects, which simply multiply all Moran influences by the same timescale-dependent non-negative quantity, not altering their relative importance or sign [see (5)].

CaseB reveals how Moran effects can interact when lags are longer than 1 model time step. For CaseB, recall that  $\epsilon^{(1)}$  effects on populations were lagged by 3q but  $\epsilon^{(2)}$  effects were unlagged (Methods), so  $l_{e1} = 3q$  and  $l_{e2} = 0q$  in the language of Fig. 2. As for CaseA, because  $(\epsilon^{(1)}, \epsilon^{(2)})$  was a white noise process for CaseB,  $l_n = 0$ , so the environmental effect alignment measure is 3q. Interaction effects were again negative on short timescales ( $\sigma = 0.5y = 2q$ ; Fig. 4c, far left side of panel) because  $l_{e1} - l_{e2} + l_n = 3q$  was  $1.5\sigma$  on that timescale, and so effects of  $\epsilon^{(1)}$  and  $\epsilon^{(2)}$  were in a half-phase relationship and counteracted each other. Similar to CaseA,  $l_{e1} - l_{e2} + l_n = 3q$  was again negligible compared to long timescales, so interaction effects were positive on long timescales (Fig. 4c, right side of panel), though timescales had to be a bit longer than in CaseA for this approximation to be as good (compare the rates at which the dashed lines level off in Fig. 4a, c). The quantity  $l_{e1} - l_{e2} + l_n = 3q$  exactly equaled the timescale for  $\sigma = 3q = 0.75y$  and equaled half the timescale for  $\sigma = 6q = 1.5y$ , hence interaction effects were, respectively, positive and negative for these timescales (Fig. 4c).

CaseA and CaseB assumed white noise processes, and therefore  $l_n$  was zero. But CaseC illustrates what can happen when noise processes have lagged associations, e.g. both processes oscillate with annual periodicity and distinct phenology, an important scenario because seasonality is common. Recall that, for CaseC,  $\epsilon^{(1)}$  effects on populations were positive and lagged by 1q, i.e.  $l_{e1} = 1$  in the language of the Supporting information analogue of Fig. 2; whereas  $\epsilon^{(2)}$  effects were unlagged and negative, i.e.  $l_{e2} = 0$  (Methods). We compare CaseC to the  $\beta$  scenarios in the Supporting information analogue of Fig. 2 instead of the  $\alpha$  scenarios of Fig. 2 itself because  $\epsilon^{(2)}$  effects were negative for CaseC, the situation considered by the  $\beta$  scenarios. For CaseC1, peaks in the periodic noise process  $\epsilon^{(1)}$  were set up to lag peaks in the periodic process  $\epsilon^{(2)}$  by 1q (Methods, Fig. 4), so that  $l_n = 1$ . Thus the environmental effect alignment measure,  $l_{e1} - l_{e2} + l_n$ , equals  $2q = 0.5y$ , and, on annual timescales, lags compounded, similar to panels c, d of the Supporting information analogue of Fig. 2: the annual positive population

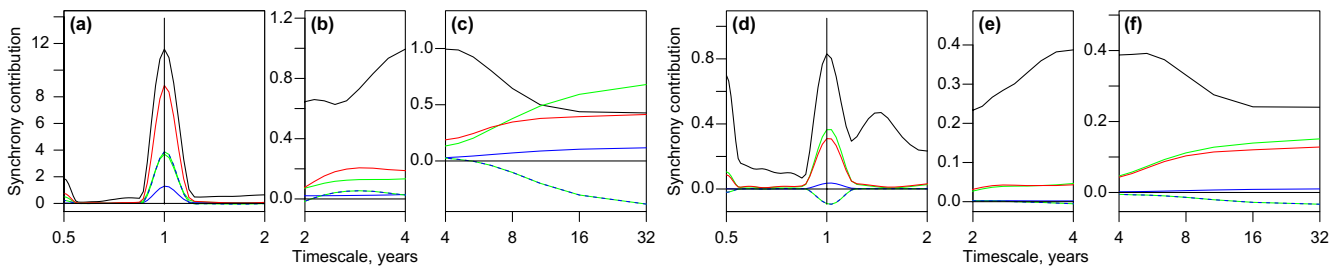


Figure 5. The new theory as applied to kelp, central CA 1 (CCA1) region (a–c) and Santa Barbara (SB) region (d–f). Panels show the terms on the right side of (5). Green lines show  $\frac{|f_{p^{(1)}}|^2}{|f_B|^2} \rho_{\varepsilon^{(1)} \varepsilon^{(1)}}$ , quantifying kelp population synchrony due to the direct Moran effects of  $\varepsilon^{(1)}$ , which, in this context, is nitrates. The blue line is  $\frac{|f_{p^{(2)}}|^2}{|f_B|^2} \rho_{\varepsilon^{(2)} \varepsilon^{(2)}}$ , quantifying kelp population synchrony due to the direct Moran effects of  $\varepsilon^{(2)}$ , which, in this context, is waves. The dashed green-blue line is  $\frac{2\text{Re}(f_{p^{(1)}} \overline{f_{p^{(2)}}} \rho_{\varepsilon^{(1)} \varepsilon^{(2)}})}{|f_B|^2}$ , which is population synchrony due to interacting Moran effects. The red line is the sum of the green, blue and green-blue lines, and is the portion of synchrony explained by nitrates, waves, and their interactions. Explained synchrony does not equal total kelp synchrony (black line) because other, unmeasured factors also help synchronize kelp dynamics. The timescale bands 0.5–2, 2–4, and >4 are separated on different panels because of the very different y-axis ranges. The CCA1 results approximately parallel the results for theoretical case study C scenario 1 (Fig. 4e; text for details). See Supporting information for the central CA 2 (CCA2) region, for which results were substantially the same as for CCA1. This figure used kelp lag  $n=4$  [see (1)]; see analogue figures in Supporting information for  $n=8, 12$ . See the online version for color renderings of all figures.

effects of  $\varepsilon^{(1)}$  were exactly  $2q$  offset from the annual negative effects of  $\varepsilon^{(2)}$ , one quarter because of the lag of  $\varepsilon^{(1)}$  peaks behind  $\varepsilon^{(2)}$  peaks, and one additional quarter because of the delayed influence of  $\varepsilon^{(1)}$  peaks on populations. This produced reinforcing interactions between the Moran effects of  $\varepsilon^{(1)}$  and  $\varepsilon^{(2)}$  on annual timescales, as reflected by our theory (Fig. 4e, f). Contrastingly, for CaseC2, peaks in the periodic noise process  $\varepsilon^{(2)}$  were set up to lag peaks in the periodic process  $\varepsilon^{(1)}$  by  $1q$ , so that  $l_n = -1$ . Thus  $l_{e1} - l_{e2} + l_n = 0$  and, on annual timescales, lags cancelled, similar to panels a, b of the Supporting information analogue of Fig. 2: the annual positive population effects of  $\varepsilon^{(1)}$  coincided with the negative effects of  $\varepsilon^{(2)}$  every year, because  $\varepsilon^{(1)}$  peaks came  $1q$  ahead of  $\varepsilon^{(2)}$  peaks each year, but population influences of  $\varepsilon^{(1)}$  were delayed by  $1q$ . This produced negative interactions between the Moran influences of  $\varepsilon^{(1)}$  and  $\varepsilon^{(2)}$  on annual timescales, as also reflected by our theory (Fig. 4g, h). On long timescales, interactions were the same for C1 and C2, and were negative, because, on those timescales, sub-annual lags make negligible difference, and the effects of  $\varepsilon^{(1)}$  on populations were positive and those of  $\varepsilon^{(2)}$  were negative.

### Illustrating properties of Moran interactions: kelp examples

We now apply our theory to kelp, fulfilling goal G3 of the Introduction. Kelp results confirm the earlier theoretical results, based on our case studies (text above and Fig. 4), that interaction effects between Moran drivers: 1) can be comparable in strength to direct Moran effects; 2) can be either

synergistic or destructive; and 3) can depend strongly on timescale. First, for all of our regions and for essentially all timescales, the magnitude of interaction effects was comparable to that of direct Moran effects (Fig. 5 for the CCA1 and SB regions and Supporting information for the CCA2 region). Second, interaction effects could be positive (e.g. annual timescales, CCA1 region on Fig. 5a), or negative (e.g. annual timescales, SB region on Fig. 5d; or long timescales >8y for either region, Fig. 5c, f). Finally, interactions depended on timescale, e.g. for CCA1 they were positive on annual timescales (Fig. 5a) and negative on timescales >8y (Fig. 5c).

### Direct Moran effects in the kelp examples

Direct Moran effects for kelp and how they manifest in our theory are fairly straightforward. Nitrates are henceforth identified with  $\varepsilon^{(1)}$  and waves with  $\varepsilon^{(2)}$ . Both nitrates and waves fluctuate seasonally in CA (Schiel and Foster 2015). Thus nitrate and wave synchrony had a strong annual component (Fig. 6a, b, j, k for the CCA1 and SB regions, Supporting information for CCA2), which produced some of the annual synchrony observed in kelp (Fig. 5a, d, green and blue lines). Nitrates and waves are also synchronous on long timescales >8y (Fig. 6g, h, p, q for the CCA1 and SB regions, Supporting information for CCA2), possibly due to the North Pacific Gyre Oscillation (DiLorenzo et al. 2008, Castorani et al. 2022). The long-timescale synchrony in nitrates and waves produced some of the long-timescale synchrony in kelp (Fig. 5c, f, green and blue lines). Kelp synchrony was stronger in CCA1 than in SB (Fig. 5a–c).

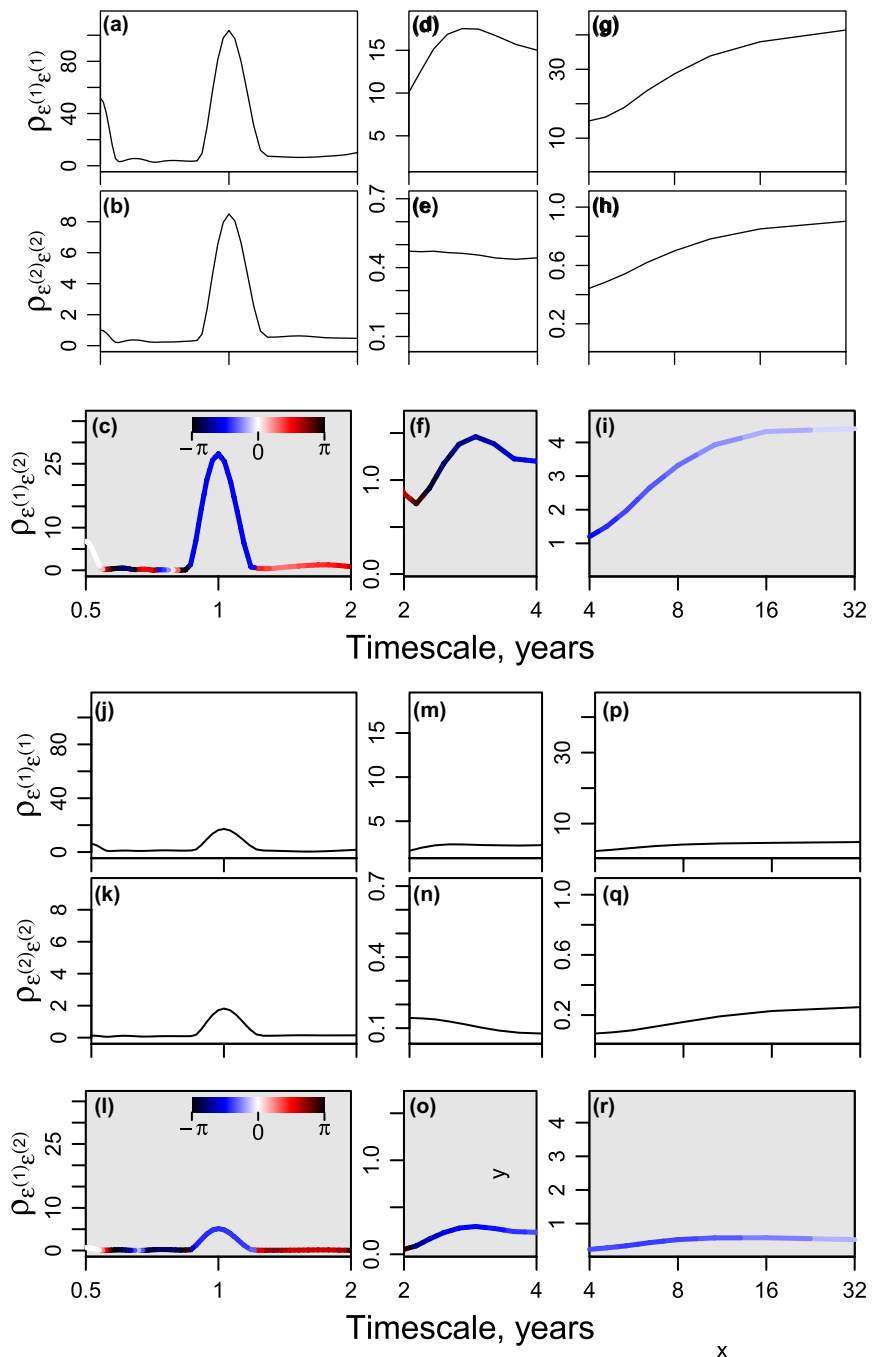


Figure 6. Synchrony and cross synchrony between environmental variables influencing kelp for CCA1 (a–i) and SB (j–r). Nitrates are identified with  $e^{(1)}$  and waves with  $e^{(2)}$ . Vertical axis extents are the same for corresponding panels for the two regions, to facilitate comparisons. Cross synchrony is complex valued, with magnitude plotted on the vertical axis and phase displayed using color. See Supporting information for CCA2, for which results were similar to CCA1. This figure used kelp lag  $n=4$ ; see analogue figures in Supporting information for  $n=8$  and 12. See the online version for color renderings of all figures.

versus d–f, black lines) in part because the synchrony of nitrates, and of waves, was more pronounced in CCA1 than in SB (Fig. 6), and also because waves had a stronger influence on kelp in central California than in SB: regression coefficients determining  $f_{p^{(1)}}$ ,  $f_{p^{(2)}}$  and  $f_B$  are in the Supporting information.

### Building intuition for Moran interactions: kelp examples

Interactions between Moran effects in CCA1 were parallel to one of the theoretical case studies, CaseC1. In CCA1, nitrates had 1q-delayed positive effects on observed kelp populations

and waves had immediate negative effects (Cavanaugh et al. 2011, Bell et al. 2015, Schiel and Foster 2015), just as  $\epsilon^{(1)}$  effects in CaseC1 were positive and delayed by 1q and  $\epsilon^{(2)}$  effects were negative and immediate. The delayed effects of nitrates in CCA1 are reflected in the tabulated regression results of Supporting information, where results for  $p_0^{(1)}$  are close to zero and those for  $p_1^{(1)}$  are positive. Immediate negative effects of waves in CCA1 are also reflected in the same Supporting information table, where entries for  $p_1^{(2)}$  are negative. Nitrate effects on kelp are probably delayed by a quarter in central CA because winter waves commonly remove kelp, and it takes time for kelp to grow to the surface and become detectable by satellite, only then revealing the effects of elevated nitrates (Cavanaugh et al. 2011, Bell et al. 2015, Schiel and Foster 2015). In CCA1, annual peak nitrates tend to come in spring, whereas annual peak waves tend to come in winter (Bell et al. 2015, Schiel and Foster 2015). Thus annual nitrate peaks tend to lag annual wave peaks by 1q, just as  $\epsilon^{(1)}$  peaks lagged  $\epsilon^{(2)}$  peaks by 1q in CaseC1. For CCA1, this is reflected in Fig. 6c, which shows that  $\rho_{\epsilon^{(1)}\epsilon^{(2)}}$  has a phase of about  $-\pi/2$  at the annual timescale. Thus  $l_{\epsilon 1}=1q$ ,  $l_{\epsilon 2}=0q$ ,  $l_n=1q$ , and so the environmental effect alignment measure is  $l_{\epsilon 1}-l_{\epsilon 2}+l_n=2q$ . Lags compound on the annual timescale, in the CCA1 case as in CaseC1: the annual positive effects of nitrates on kelp tend to come in summer, and the annual negative effects of waves come in winter, producing reinforcing interactions between Moran effects. Interactions between Moran effects on long-timescales ( $>8y$ ) were also similar for both CCA1 and CaseC1 (compare Fig. 4e, 5c), and for the same reason in both cases: on long timescales, sub-annual lags are inconsequential, and the positive effects of nitrates/ $\epsilon^{(1)}$  and the negative effects of waves/ $\epsilon^{(2)}$  therefore lead to negative interactions. Interactions between Moran effects in CCA2 operated similarly to CCA1 (Supporting information).

Due to different nitrate effects on observable kelp growth in SB compared to CCA1, interactions between Moran effects followed a different mechanism in SB compared to CCA1, leading to the slightly negative versus positive interactions already documented on annual timescales for the two regions (Fig. 5d versus a). Whereas in CCA1, nitrate effects on observed kelp density were delayed by 1q, in SB nitrate effects were observable within the same quarter: see the tabulated regression results of Supporting information, where  $p_0^{(1)}$  terms were close to zero for CCA1 and positive for SB, whereas  $p_1^{(1)}$  terms were positive for CCA1 and close to zero for SB. Wave effects were negative and immediate in both regions, i.e.  $\rho_0^{(2)} < 0$  in the same Supporting information table. In southern CA, kelp is less likely to be completely removed by winter waves (Reed et al. 2011). Effects of elevated nitrates on the growth of kelp stands already reaching the surface can be observed within the quarter (Cavanaugh et al. 2011, Bell et al. 2015, Schiel and Foster 2015). Annual peaks in nitrates still tended to lag annual peaks in waves by 1q in SB, as in CCA1, though the seasonal periodicity of both variables was reduced in SB compared to CCA1 (Fig. 6l versus c). Thus, in SB, the environment effect alignment measure

was 1q, contrasting with its value of 2q in CCA1. Whereas in CCA1, the tendency of nitrate annual peaks to follow wave annual peaks by 1q, together with the tendency of nitrate effects on kelp to be delayed by 1q, resulted in summer positive nitrate effects and winter negative wave effects which reinforced synchrony; in SB nitrate instead both peaked and had its positive effects on kelp in spring, while waves still had negative effects on kelp in winter. Thus the effects of nitrates and waves in SB were approximately a quarter-cycle separated from each other with respect to the annual timescale, and so produced neither much reinforcement nor much destructive interference of synchrony on annual timescales (Fig. 5d). Slightly negative interactions were observed (Fig. 5d) because of slight deviations from the approximate phase alignments described above. On long timescales, interactions between Moran effects were analogous in CCA1 and SB (though weaker in SB; Fig. 5c versus f) because, again, sub-annual lags are inconsequential on long timescales and what mattered instead was the oppositely signed influences of the two environmental variables.

## Discussion

We provided a general mathematical theory of the new mechanism of interactions between Moran effects. When two related spatially synchronous environmental drivers both influence a set of populations across a landscape, interactions can make synchrony in the populations either substantially stronger or markedly weaker than would otherwise be expected. Our general theory illuminates precisely how timings of influences of the drivers on populations can interact with relationships between the drivers to alter Moran effects. Interactions may vary by timescale in both their strength and sign. We used our theory and several case studies based on models and kelp populations to provide intuition about the new mechanism. Because Moran effects are ubiquitous and interactions between Moran effects were detected on both of the two occasions they have been tested for (Sheppard et al. 2019, Castorani et al. 2022), interactions may be common (see also below). Moran interactions are therefore a newly recognized and potentially widespread aspect of a fundamental means (Moran effects) by which environmental factors influence populations and diverse, synchrony-related phenomena such as ecosystem stability (Wilcox et al. 2017), population cycling (Anderson et al. 2021), and extinction (Ghosh et al. 2020c). Climate change is altering many aspects of environmental variables, including their means, variances, and spatial correlations (Lyon et al. 2019, Keelings and Moradkhani 2020), as well as relationships between environmental variables and the nature of their influences on populations. There is therefore also potential for climate change to alter interactions between Moran effects, in ways our new theory may help researchers to understand. The augmented fundamental understanding of Moran effects which we have provided may substantially benefit both basic (Liebhold et al.

2004) and applied (Hansen et al. 2020, Larsen et al. 2021, Herfindal et al. 2022) ecological research (see also below).

We argue that it is likely that interactions between Moran effect are common. Most species are influenced by more than one environmental driver. Drivers are frequently spatially autocorrelated, and are also often related to each other because of their common origin in underlying climatic phenomena such as the North Pacific Gyre Oscillation (NPGO) or El Niño Southern Oscillation (ENSO). Driver pairs which may commonly produce interacting Moran effects include instances where the same quantity is measured in distinct parts of the year (e.g. spring and summer temperatures, or March and April rainfall); or when distinct variables are measured in the same part of the year (e.g. spring temperature and precipitation). Such scenarios involving seasonality of effects, which were recently explored by Walter et al. (2023), can produce specific manifestations of the general mechanisms explored here. Walter et al. (2023) found interactions and cross synchrony to be important. Future work should systematically investigate cross synchrony ( $\rho_{\varepsilon^{(1)}\varepsilon^{(2)}}$ ) of environmental variables. Temperature and precipitation variables measured in the same season may be particularly important candidates for interactions because of the well-known joint influence of these variables on plants.

We again revisit the intuition behind interacting Moran effects using the central CA kelp example as a vehicle. Large winter waves have immediate negative effects on kelp in central CA, whereas the positive effects of spring nitrates manifest in summer. So nutrient and wave effects can reinforce each other in producing annual oscillations: large kelp increases in summer due to abundant nutrients can be followed by big crashes in winter due to waves, both factors combining to accentuate the annual cycle. Thus positive interactions between Moran effects on annual timescales occur whenever years with above-average waves coincide with years with plentiful nutrients in other locations: if a large-wave year in location A coincides with a high-nutrient year in location B, both locations will tend to have bigger annual fluctuations that year, accentuating annual-timescale synchrony between the locations (Castorani et al. 2022). Sub-annual lags and delays make essentially no difference, however, on long timescales. On long timescales, large-wave and abundant-nutrient years counteract each other: if a multi-year period of large waves in location A coincides with a multi-year period of abundant nutrients in location B, the multi-year-average kelp abundance in A will tend to be reduced, whereas the multi-year-average kelp abundance in B will tend to be augmented, reducing long-timescale synchrony. Lags and interactions between drivers must always be compared to the timescale of interest to determine interaction effects, as in Fig. 2 and its analogue in Supporting information, and as captured formally in our theory. Thus interactions between Moran effects provide yet another reason, among many reasons previous work has already documented (Vasseur and Gaedke 2007, Keitt 2008, Vasseur et al. 2014, Sheppard et al. 2016, Defriez et al. 2016, Defriez and Reuman 2017a, b, Walter et al. 2017, Desharnais et al. 2018, Zhao et al. 2020, Anderson et al.

2021), that patterns of synchrony must be considered from a timescale-specific viewpoint for full understanding.

Our results about kelp were consistent with those of Castorani et al. (2022), though that study uses distinct methods. In spite of numerous methodological choices which differed between the two studies, both our results and those of Castorani et al. (2022) show positive effects of both nutrients and waves on synchrony on both annual and long (>4y) timescales in both central and southern CA. And both studies show positive interactions between nutrient and wave Moran effects on annual timescales in central CA, but negative interactions in southern CA on annual timescales and in both central and southern CA on long timescales. As stated in the Introduction, our results about kelp were not intended to reveal new aspects of kelp ecology – we did that already in Castorani et al. (2022) – instead our purpose was to use kelp as a vehicle for helping explain the mechanism of interacting Moran effects. Kelp is a good vehicle for this purpose because of the clarity of the lagged effects in the kelp system, and the differences in the lags between southern and central CA.

Since both our Fourier approach and the wavelet methods of Castorani et al. (2022) provided similar results when applied to kelp, when should one approach be applied in favor of the other? The Fourier approach of our study was designed to facilitate mathematical examination of interactions between Moran effects as a general mechanism, and development of general theory. The Fourier approach facilitates deriving analytic results from mathematical models such as (4). The wavelet approach of Castorani et al. (2022) was instead optimized for detecting interactions and identifying Moran mechanisms in data, in spite of non-stationarity and other complicating features which are present in many ecological datasets. The study of Sheppard et al. (2019) developed the wavelet methods applied by Castorani et al. (2022); an open-source implementation of these methods (Reuman et al. 2021) can facilitate future work. The modelling approach of this study relates indirectly to the approach of Anderson et al. (2021), though that study concerned different research questions.

It has been a frequent topic of research why populations are often less synchronous, or synchronous over a smaller spatial extent, than might be expected given the strength and extent of synchrony of an environmental driver (Herfindal et al. 2022). Our new mechanism of interacting Moran effects provides both a new means by which populations may be less synchronous than population drivers; and also a new means by which populations can be more synchronous than environmental drivers. Previously known mechanisms by which populations can be less synchronous than environmental drivers include demographic stochasticity and measurement error. Antagonistic interactions between Moran drivers may be a common and previously unrecognized additional mechanism contributing to this discrepancy. On the other hand, two recent papers described ‘enhanced Moran effects’ by which specific patterns of temporal autocorrelation in Moran drivers can theoretically cause greater synchrony in populations than in drivers (Massie et al. 2015, Desharnais et al. 2018).

Synergistic interaction between Moran drivers is another mechanism by which populations can be more synchronous than expected.

Our model is a linear population dynamical model, but most population dynamics are probably nonlinear, at least to some degree. We speculate on what may be the outcome if future work explores interactions between two or more Moran effects using nonlinear population dynamical models. Some researchers have explored Moran effects of one environmental variable acting on nonlinear population models and found generally that synchronous environmental fluctuations tend to promote synchronous population fluctuations, in spite of nonlinearities, though often to a lesser degree than for the linear case (Engen and Saether 2005, Royama 2005). Our model is a linearization of a very general population dynamical model [Supporting information section S1.2 of Desharnais et al. (2018) and Supporting information section S1 of Walter et al. (2017)], and it is well known that analytic results for linearized models such as we have developed also hold, approximately, for the original nonlinear model, as long as the noise impinging the model is sufficiently weak. How weak is ‘sufficiently weak’ is model dependent, but prior work examining that question provided evidence that weak noise approximations using linearizations of commonly used ecological models are often actually quite accurate, even for fairly strong noise (Nisbet et al. 1977). Therefore we speculate that our main observations will hold even for nonlinear systems: 1) Moran effects can substantially interact, either synergistically or destructively; 2) interactions can depend on timescale; and 3) the nature of effects depends on relative, timescale-specific lags of environmental influences on populations and between environmental variables. However, future work should nevertheless examine Moran interactions and nonlinear models, since much has been learned by exploring deviations of ecological models from predictions of theory based on linearization (Reuman et al. 2006).

A better understanding of fundamental ecological phenomena can be used to improve conservation efforts. But how, specifically, might improved understanding of Moran effects from this study aid kelp conservation or restoration? Scientists and managers are currently developing a stability model that informs when, where, and how to restore kelp forests following recent large-scale declines (Bell et al. 2023). Specifically, these efforts inform kelp restoration by modelling the dynamics of kelp abundance (measured by diver surveys) as a function of environmental and bathymetric variables. Resulting maps of kelp stability are then compared to maps of recent canopy declines to identify sites where restoration activities are needed and would lead to stable future forests (Giraldo-Ospino et al. In prep.). It is well known that stability of regional populations is influenced by synchrony, both generally (Wilcox et al. 2017) and for kelp specifically (Walter et al. 2022); and the first step in the emerging kelp restoration decision tree of Bell et al. (2023) and Giraldo-Ospino et al. (In prep.) involves predicting kelp stability across all suitable habitat in California. Future iterations of

this process may consider interacting Moran effects to better predict stability and thereby better support kelp restoration.

Climate change has the potential to influence interactions between Moran effects in two specific ways which can be illuminated by our theory, and this potential should be investigated in future work. Examining the third term of (5), climate change could alter interaction effects if it: 1) alters the term  $\rho_{\varepsilon^{(1)}\varepsilon^{(2)}}$  quantifying cross synchrony between Moran drivers; or 2) alters one of the terms  $f_{\mathcal{P}^{(1)}}$  or  $f_{\mathcal{P}^{(2)}}$  specifying the nature of the influence of the environmental variables  $\varepsilon^{(1)}$  and  $\varepsilon^{(2)}$ , respectively, on populations. As advocated above, the term  $\rho_{\varepsilon^{(1)}\varepsilon^{(2)}}$  should be systematically computed in future work, for a variety of environmental variables, to assess whether interactions between Moran effects are likely to be general. As part of that process, the potential for changes in  $\rho_{\varepsilon^{(1)}\varepsilon^{(2)}}$  could also be assessed, by using either time-windowed versions or wavelet adaptations of this statistic, applied to either long-term climate records or future climate scenarios. Differences in  $f_{\mathcal{P}^{(1)}}$  were responsible for differences in the nature of Moran interactions between central CA and southern CA (Results), specifically differences between the two regions in the lag of nitrate effects on kelp populations. If climate change modifies environmental effects on populations in a related way it would be expected to produce similarly large changes in Moran interactions. Climate change may alter lags and delays associated with environmental effects on populations in at least two ways: 1) by altering species phenology; and 2) by increasing or decreasing growth rates and thereby decreasing or increasing delays. Though it is too early to conclude that effects on Moran interactions are among the most important impacts of climate change, we feel the mechanisms outlined above are sufficient to warrant further investigation.

We have focused on interactions between two Moran drivers, but synchrony in most systems may be a phenomenon with multiple (more than two) interacting causes. Kendall et al. (2000) considered interactions between dispersal and a Moran mechanism of synchrony. Their research questions were therefore distinct from ours, but combining their viewpoints and ours may lead to future work about interactions between dispersal and more than one Moran driver of synchrony. Although we considered only two Moran drivers in our theory and examples, essentially all population systems are influenced by multiple environmental drivers, and environmental drivers very commonly are associated with large-scale climatic phenomena such as ENSO, and hence are associated with each other. Thus it may be quite common for synchrony to simultaneously be caused by dispersal and multiple distinct Moran effects, and these influences may interact in multifarious combinations. It may be necessary in future work to consider interactions between dispersal and two Moran drivers. It may be useful to consider cases for which multiple related Moran drivers all interact. Dispersal can readily be added to our modelling framework: Desharnais et al. (2018) performed a spectral analysis on a model similar to ours which

included dispersal. Future work should consider whether and when scenarios of multi-driver interactions between causes of synchrony can lead to synchrony patterns which differ fundamentally from what one would expect from one or two mechanisms. Potential interactions increase as the square of the number of drivers, so interactions seem likely to become more important as our viewpoint of synchrony expands.

**Acknowledgements** – This project used data developed through the Santa Barbara Coastal Long Term Ecological Research project, funded through NSF-OCE award 1831937. The authors thank Vadim Karatayev, Maowei Liang, Kyle Emery, Nat Coombs, Adeola Adeboje, and Ethan Kadiyala for helpful discussions.

**Funding** – This study was partly funded by the U.S. National Science Foundation (NSF) through linked NSF-OCE awards 2023555, 2023523, 2140335, and 2023474 to M.C.N.C, K.C.C., T.W.B., and D.C.R., respectively; by NSF-Math Bio award 1714195 to D.C.R.; and by support to D.C.R. from the James S. McDonnell Foundation, the Humboldt Foundation, and the California Department of Fish and Wildlife Delta Science Program.

## Author contributions

**Daniel C. Reuman:** Conceptualization (lead), formal analysis (lead), funding acquisition (equal), investigation (lead), methodology (lead), project administration (equal), resources (lead), software (lead), validation (lead), visualization (lead), writing - original draft (lead), writing - review and editing (lead). **Max C. N. Castorani:** Conceptualization, data curation, funding acquisition (equal), project administration (equal), visualization, writing - original draft, writing - review and editing. **Kyle C. Cavanaugh:** Data curation, funding acquisition (equal), writing - review and editing. **Lawrence W. Sheppard:** Conceptualization, formal analysis, funding acquisition (equal), methodology, writing - review and editing. **Jonathan A. Walter:** Conceptualization, formal analysis, funding acquisition (equal), methodology, project administration (equal), writing - review and editing. **Tom W. Bell:** Data curation (lead), funding acquisition (equal), writing - review and editing.

## Transparent peer review

The peer review history for this article is available at <https://publons.com/publon/10.1111/ecog.06795>.

## Data availability statement

The empirical portions of this study were based on existing data which had already been published at <https://doi.org/10.6073/pasta/27e795dee803493140d6a7cdc3d23379>.

## Supporting information

The Supporting information associated with this article is available with the online version.

## References

- Abbott, K. 2007. Does the pattern of population synchrony through space reveal if the Moran effect is acting? – *Oikos* 199: 903–912.
- Allstadt, A., Liebhold, A., Johnson, D., Davis, R. and Haynes, K. 2015. Temporal variation in the synchrony of weather and its consequences for spatiotemporal population dynamics. – *Ecology* 96: 2935–2946.
- Anderson, T., Walter, J., Levine, T., Hendricks, S., Johnston, K., White, D. and Reuman, D. 2018. Using geography to infer the importance of dispersal for the synchrony of freshwater plankton. – *Oikos* 127: 403–414.
- Anderson, T., Sheppard, L., Walter, J., Rolley, R. and Reuman, D. 2021. Synchronous effects produce cycles in deer populations and deer-vehicle collisions. – *Ecol. Lett.* 24: 337–347.
- Bell, T., Cavanaugh, K., Reed, D. and Siegel, D. 2015. Geographical variability in the controls of giant kelp biomass dynamics. – *J. Biogeogr.* 42: 2010–2021.
- Bell, T., Cavanaugh, K., Reuman, D., Castorani, M., Sheppard, L. and Walter, J. 2021. SBC LTER: *REEF: Macrocystis pyrifera* biomass and environmental drivers in southern and central California, ver. 1. – <https://doi.org/10.6073/pasta/27e795dee803493140d6a7cdc3d23379>.
- Bell, T., Cavanaugh, K., Saccocciano, V., Cavanaugh, K., Housekeeper, H., Eddy, N., Schuetzenmeister, F., Rindlaub, N. and Gleason, M. 2023. Kelpwatch: a new visualization and analysis tool to explore kelp canopy dynamics reveals variable response to and recovery from marine heatwaves. – *PLoS One* 18: e0271477.
- Bogdziewicz, M., Hacket-Pain, A., Ascoli, D. and Szymkowiak, J. 2021. Environmental variation drives continental-scale synchrony of European beech reproduction. – *Ecology* 102: e03384.
- Brillinger, D. 2001. Time series: data analysis and theory, Classics edn. – Society for Industrial and Applied Mathematics.
- Castorani, M., Bell, T., Walter, J., Reuman, D., Cavanaugh, K. and Sheppard, L. 2022. Disturbance and nutrients synchronize kelp forests across scales through interacting Moran effects. – *Ecol. Lett.* 25: 1854–1868.
- Cavanaugh, K., Siegel, D., Reed, D. and Dennison, P. 2011. Environmental controls of giant kelp biomass in the Santa Barbara Channel, California. – *Mar. Ecol. Prog. Ser.* 429: 1–17.
- Cavanaugh, K., Kendall, B., Siegel, D., Reed, D., Alberto, F. and Assis, J. 2013. Synchrony in dynamics of giant kelp forests is driven by both local recruitment and regional environmental controls. – *Ecology* 94: 499–509.
- Defriez, E. and Reuman, D. 2017a. A global geography of synchrony for marine phytoplankton. – *Global Ecol. Biogeogr.* 26: 867–877.
- Defriez, E. and Reuman, D. 2017b. A global geography of synchrony for terrestrial vegetation. – *Global Ecol. Biogeogr.* 26: 878–888.
- Defriez, E., Sheppard, L., Reid, P. and Reuman, D. 2016. Climate-change-related regime shifts have altered spatial synchrony of plankton dynamics in the North Sea. – *Global Change Biol.* 22: 2069–2080.
- Desharnais, R., Reuman, D., Costantino, R. and Cohen, J. 2018. Temporal scale of environmental correlations affects ecological synchrony. – *Ecol. Lett.* 21: 1800–1811.
- DiLorenzo, E., Schneider, N., Cobb, C., Franks, P., Chhak, K., Miller, A., McWilliams, J., Bograd, S., Arango, H., Curchitser, E. 2018. The role of the Southern Ocean in the global geography of synchrony. – *Global Ecol. Biogeogr.* 27: 103–113.

- E. and Powell, T. 2008. North Pacific gyre oscillation links ocean climate and ecosystem change. – *Geophys. Res. Lett.* 35: L08607.
- Engen, S. and Saether, B.-E. 2005. Generalizations of the Moran effect explaining spatial synchrony in population fluctuations. – *Am. Nat.* 166: 531–642.
- Ghosh, S., Sheppard, L., Holder, M., Loecke, T., Reid, P., Bever, J. and Reuman, D. 2020a. Copulas and their potential for ecology. – *Adv. Ecol. Res.* 62: 409–468.
- Ghosh, S., Sheppard, L., Reid, P. and Reuman, D. 2020b. A new approach to interspecific synchrony in population ecology. – *Ecol. Evol.* 10: 12764–12776.
- Ghosh, S., Sheppard, L. and Reuman, D. 2020c. Tail associations in ecological variables and their impact on extinction risk. – *Ecosphere* 11: e03132.
- Giraldo-Ospino, A., Bell, T., Carr, M. and Caselle, J. In prep. Classification scheme to prioritize sites for kelp restoration.
- Gouveia, A. R., Bjørnstad, O. N. and Tkadlec, E. 2016. Dissecting geographic variation in population synchrony using the common vole in central Europe as a test bed. – *Ecol. Evol.* 6: 212–218.
- Grenfell, B., Wilson, K., Finkenstädt, B., Coulson, T., Murray, S., Albon, S., Pemberton, J., Clutton-Brock, T. and Crawley, M. 1998. Noise and determinism in synchronized sheep dynamics. – *Nature* 394: 674–677.
- Hansen, B., Grotan, V., Herfindal, I. and Lee, A. 2020. The Moran effect revisited: spatial population synchrony under global warming. – *Ecography* 43: 1591–1602.
- Haynes, K. and Walter, J. 2022. Advances in understanding the drivers of population spatial synchrony. – *Curr. Opin. Insect Sci.* 53: 100959.
- Haynes, K., Bjørnstad, O., Allstadt, A. and Liebhold, A. 2013. Geographical variation in the spatial synchrony of a forest-defoliating insect: isolation of environmental and spatial drivers. – *Proc. R. Soc. B* 280: 20122373.
- Haynes, K., Walter, J. and Liebhold, A. 2019. Population spatial synchrony enhanced by periodicity and low detuning with environmental forcing. *Proc. R. Soc. B* 286: 20182828.
- Herfindal, I., Lee, A., Marquez, J., LeMoulliec, M., Peeters, B., Hansen, B., Henden, J.-A. and Saether, B.-E. 2022. Environmental effects on spatial population dynamics and synchrony: lessons from northern ecosystems. – *Clim. Res.* 86: 113–123.
- Keelings, D. and Moradkhani, H. 2020. Spatiotemporal evolution of heat wave severity and coverage across the United States. – *Geophys. Res. Lett.* 47: e2020GL087097.
- Keitt, T. 2008. Coherent ecological dynamics induced by large-scale disturbance. – *Nature* 454: 331–334.
- Kendall, B. E., Bjørnstad, O. N., Bascompte, J., Keitt, T. H. and Fagan, W. F. 2000. Dispersal, environmental correlation, and spatial synchrony in population dynamics. – *Am. Nat.* 155: 628–636.
- Koenig, W., Knops, J., Pesendorfer, M., Zaya, D. and Ashley, M. 2017. Drivers of acorn production in the valley oak (*Quercus lobata*) at two spatial scales. – *Ecology* 98: 3056–3062.
- Larsen, S., Comte, L., Filipe, A., Fortin, M.-J., Jacquet, C., Ryser, R., Tedesco, P., Brose, U., Eros, T., Giam, X., Irving, K., Ruhi, A., Sharma, S. and Olden, J. 2021. The geography of metapopulation synchrony in dendritic river networks. – *Ecol. Lett.* 24: 791–801.
- Liebhold, A., Koenig, W. D. and Bjørnstad, O. N. 2004. Spatial synchrony in population dynamics. – *Annu. Rev. Ecol. Evol. Syst.* 35: 467–490.
- Lyon, B., Barnston, A., Coffel, E. and Horton, R. 2019. Projected increase in the spatial extent of contiguous US summer heat waves and associated attributes. – *Environ. Res. Lett.* 14: 114029.
- Massie, T., Weithoff, G., Kucklander, N., Gaedke, U. and Blasius, B. 2015. Enhanced Moran effect by spatial variation in environmental autocorrelation. – *Nat. Commun.* 6: 5993.
- Moran, P. 1953. The statistical analysis of the Canadian lynx cycle. II Synchronization and meteorology. – *Aus. J. Zool.* 1: 291–298.
- Nisbet, R., Gurney, W. and Pettipher, M. 1977. An evaluation of linear models of population fluctuations. – *J. Theor. Biol.* 68: 143–160.
- Ranta, E., Kaitala, V. and Lindstrom, J. 1999. Spatially autocorrelated disturbances and patterns in population synchrony. – *Proc. R. Soc. Lond. B* 266: 1851–1856.
- Reed, D., Rassweiler, A., Carr, M., Cavanaugh, K., Malone, D. and Siegel, D. 2011. Wave disturbance overwhelms top-down and bottom-up control of primary production in California kelp forests. – *Ecology* 92: 2108–2116.
- Reuman, D., Desharnais, R., Costantino, R., Ahmad, O. and Cohen, J. 2006. Power spectra reveal the influence of stochasticity on nonlinear population dynamics. *Proc. Natl. Acad. Sci. USA* 103: 18860–18865.
- Reuman, D., Anderson, T., Walter, J., Zhao, L. and Sheppard, L. 2021. *wsyn*: wavelet approaches to studies of synchrony in ecology and other fields. – <https://cran.r-project.org/web/packages/wsyn/index.html>.
- Royama, T. 2005. Moran effect on nonlinear population processes. – *Ecol. Monogr.* 75: 277–293.
- Schiel, D. and Foster, M. 2015. The biology and ecology of giant kelp forests. – Univ. of California Press.
- Sheppard, L., Bell, J., Harrington, R. and Reuman, D.C. 2016. Changes in large-scale climate alter spatial synchrony of aphid pests. – *Nat. Clim. Change* 6: 610–613.
- Sheppard, L., Reid, P. and Reuman, D. 2017. Rapid surrogate testing of wavelet coherences. – *Eur. Phys. J. Nonlinear Biomed. Sci.* 5: 1.
- Sheppard, L., Defriex, E., Reid, P. and Reuman, D. 2019. Synchrony is more than its top-down and climatic parts: interacting Moran effects on phytoplankton in British seas. – *PLoS Comput. Biol.* 15: e1006744.
- Tedesco, P., Hugueny, B., Paugy, D. and Fermon, Y. 2004. Spatial synchrony in population dynamics of West African fishes: a demonstration of an intraspecific and interspecific Moran effect. – *J. Anim. Ecol.* 73: 693–705.
- Vasseur, D. and Gaedke, U. 2007. Spectral analysis unmasks synchronous and compensatory dynamics in plankton communities. – *Ecology* 88: 2058–2071.
- Vasseur, D. and Fox, J. 2009. Phase-locking and environmental fluctuations generate synchrony in a predator-prey community. – *Nature* 460: 1007–1010.
- Vasseur, D., Fox, J., Gonzalez, A., Adrian, R., Beisner, B., Helmus, M., Johnson, C., Kratina, P., Kremer, C., de Mazancourt, C., Miller, E., Nelson, W., Paterson, M., Rusak, J., Shurin, J. and Steiner, C. 2014. Synchronous dynamics of zooplankton competitors prevail in temperate lake ecosystems. *Proc. R. Soc. B* 281: 20140633.
- Walter, J., Sheppard, L., Anderson, T., Kastens, J., Bjørnstad, O., Liebhold, A. and Reuman, D. 2017. The geography of spatial synchrony. – *Ecol. Lett.* 20: 801–814.

- Walter, J., Sheppard, L., Venugopal, P., Reuman, D., Dively, G., Tooker, J and Johnson, D. 2019. Weather and regional crop composition variation drive spatial synchrony of lepidopteran agricultural pests. – *Ecol. Entomol.* 45: 573–582.
- Walter, J., Hallett, L., Sheppard, L., Anderson, T., Zhao, L., Hobbs, R., Suding, K. and Reuman, D. 2020. Micro-scale geography of synchrony in a serpentine plant community. – *J. Ecol.* 109: 750–762.
- Walter, J., Castorani, M., Bell, T., Sheppard, L., Cavanaugh, K. and Reuman, D. 2022. Tail-dependent spatial synchrony arises from nonlinear driver-response relationships. – *Ecol. Lett.* 25: 1189–1201.
- Walter, J., Reuman, D., Hall, K., Shugart, H. and Shoemaker, L. 2023. Seasonality in environmental and population processes alter population spatial synchrony. – *Am. Nat.*
- Wang, S. and Loreau, M. 2014. Ecosystem stability in space:  $\alpha$ ,  $\beta$  and  $\gamma$  variability. – *Ecol. Lett.* 17: 891–901.
- Wilcox, K. et al. 2017. Asynchrony among local communities stabilises ecosystem function of metacommunities. – *Ecol. Lett.* 20: 1534–1545.
- Zhao, L., Wang, S., Hallett, L., Rypel, A., Sheppard, L., Castorani, M., Shoemaker, L., Cottingham, K., Suding, K. and Reuman, D. 2020. A new variance ratio metric to detect the timescale of compensatory dynamics. – *Ecosphere* 11: e03114.